

Discovering classical spin liquids by topological search of high symmetry nets

Joseph A. M. Paddison^{1,*} and Matthew J. Cliffe^{2,†}

¹Neutron Scattering Division, Oak Ridge National Laboratory, Oak Ridge, Tennessee 37831, USA

²School of Chemistry, University Park, Nottingham, NG7 2RD, United Kingdom

(Dated: June 11, 2024)

Spin liquids are a paradigmatic example of a non-trivial state of matter, and the search for new spin liquids is a key direction of physics, chemistry, and materials science. Geometric frustration—where the geometry of the net that the spins occupy precludes the generation of a simple ordered state—is a particularly fruitful way to generate these intrinsically disordered states. A particular focus has been on a handful of high symmetry nets. There are, however, many three-dimensional nets, each of which has the potential to form unique states. In this paper, we investigate the high symmetry nets—those which are both node- and edge-transitive—for the simplest possible interaction sets: nearest-neighbour couplings of antiferromagnetic Heisenberg and Ising spins. While the well-known **crs** (pyrochlore) net is the only nearest-neighbour Heisenberg antiferromagnet which does not order, we identify two new frustrated nets (**lcx** and **thp**) that possess finite temperature Heisenberg spin-liquid states with strongly suppressed magnetic ordering and non-collinear ground states. With Ising spins, we identify four new classical spin liquids that do not order down to $T/J = 10^{-2}$. We highlight materials that contain these high symmetry nets, and which could, if substituted with appropriate magnetic ions, potentially host these unusual states. Our systematic survey will guide searches for novel magnetic phases.

I. INTRODUCTION

Frustrated magnets, where the combination of geometry and interactions suppress the emergence of long-range ordered states, are rich in unconventional magnetic states: from complex spin textures^{1,2} to spin liquids.^{3–6} However, the existence of frustration implies a (near-)degeneracy of states, and hence that the nets on which the spins are arranged must be highly symmetric. Most research on frustrated magnets has focused on a handful of the most symmetric nets: in two dimensions, the kagome (**kgm**)^{7,8} and triangular (**hxl**)^{9,10} nets, and in three, the pyrochlore (**crs**) net,^{11,12} where the degeneracy of states and hence the frustration is greatest.

Although we now understand much about the behaviour of spins arranged on these high symmetry nets, many other nets are less well understood, particularly in three dimensions. A diversity of topologies has been realised in metal-organic framework (MOF) crystals and enabled a range of functional properties, often using the pore network-topology to achieve chemical separations^{13,14}, but increasingly also for realising novel magnetic nets¹⁵. These results highlight that the synthetic chemistry need not be a barrier to moving beyond traditional nets. Determining whether a given net could host frustration-derived unconventional magnetic states is a key step towards the discovery of such states in real materials, whether through targeted ‘reticular’ design of new magnets or through computational search of known materials.¹⁶

The most important class of nets comprises those with only one symmetry independent node (vertex-transitive) and only one symmetry independent nearest-neighbour interaction (edge-transitive). Examples of these nets are shown in Fig. 1 and listed in Table I. These are the only nets in which a frustrated state can be achieved without fine-tuning, as all other nets will have at least two symmetry-inequivalent nearest-neighbour interactions. Each vertex- and edge-transitive net can generate an infinite number of other vertex- and edge-transitive nets, by connecting each node to its n th-neighbour rather than the nearest neighbour ($n = 1$); however, these higher-order

nets are rarely realised in real materials, as their highest symmetry realisations typically require intersecting edges, very high degrees of interpenetration, very long ligands, or very high coordination numbers.

In this paper, we investigate the behaviour of classical antiferromagnets of the 21 ‘simplest’ vertex- and edge-transitive 3D nets. These nets have many different names [Table I], and so to identify each net unambiguously we use the Reticular Chemistry Structural Resource (RCSR) nomenclature, where each net is assigned a three letter code written in bold.¹⁷ We restrict our study to the vertex- and edge-transitive nets generated by connecting the nodes nearest in space to each other in their highest symmetry embedding (20 nets). We also consider the **lcy** net in which next-nearest neighbour nodes are connected, because the nearest neighbour net is only 1 connected, $d_1/d_2 = 0.82$, and it has been physically realised. Further detail on these nets is available in the supporting information.^{18,19,20} Further, we focus on the simplest

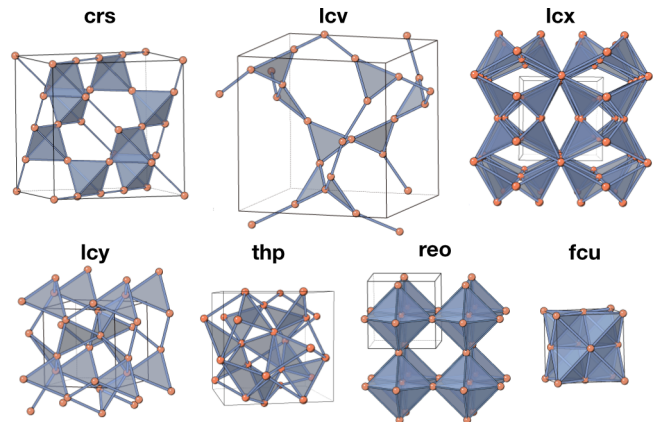


Figure 1. Vertex and edge-transitive frustrated nets in their high symmetry embeddings. For each net, the edges are the shortest node-node distance, except for **lcx** for which the edges are the next-shortest node-node distance.

arXiv:2406.06416v1 [cond-mat.str-el] 10 Jun 2024

Table I. Common names of the high symmetry topologies, coordination number z , and examples of compounds with these topologies.

	z	Synonyms	Compounds	Space Group
crs	4	pyrochlore, spinel B-site, cubic Laves	$\text{HoCHo}_2\text{Ti}_2\text{O}_7$, ²³ $\text{CrCMgCr}_2\text{O}_4$ ²⁴	$Fd\bar{3}m$
fcu	12	face-centered cubic, rocksalt, double perovskite	MnCMnO , ²⁵ $\text{IrCK}_2\text{IrCl}_6$ ²⁶	$Fm\bar{3}m$
lcv	4	hyperkagome, (half-)garnet	$\text{GdCGd}_3\text{Ga}_5\text{O}_{12}$, ²⁷ $\text{IrCNa}_4\text{Ir}_3\text{O}_8$ ²⁸	$I4_132$
lcx	8	next-nearest neighbour A15 phase	CrCCr_3Si , ²⁹ $\text{PtCNaPt}_3\text{O}_4$, ³⁰ $\text{Eu}_2\text{CEu}_8\text{Ga}_{18}\text{Ge}_{30}$ ³¹	$Pm\bar{3}n$
lcy	6	trillium ^{32,33}	$\text{MnCNaMn}(\text{HCO}_2)_3$, ¹⁵ $P4_132$ MnCMnSi ³⁴	
reo	8	octahedral, octochlore	MnCMn_3ZnN ³⁵	$Pm\bar{3}m$
thp	8	thorium phosphide	UCU_3X_4 , $\text{X}=\text{P,As,Sb,Bi}$ ³⁶	$I4\bar{3}d$

interactions, with a single antiferromagnetic interaction J that couples nearest-neighbour spins only. We consider Heisenberg $E = J \sum_{\langle i,j \rangle} \mathbf{S}_i \cdot \mathbf{S}_j$ and Ising $E = J \sum_{\langle i,j \rangle} S_i S_j$ models, where \mathbf{S}_i is a classical vector, $S_i = \pm 1$, and the summation is over all nearest-neighbour pairs (next-nearest neighbour pairs for **lcx**). While more complex interactions (*e.g.*, bond-directional exchange²¹) or multiple exchange interactions J_n ²² can also yield interesting physics, in most cases the Heisenberg interaction remains the largest and physically most relevant term.

We employ Monte Carlo simulation on large supercells to provide an overview of the magnetic properties for these high-symmetry nets, and to calculate quantities that can be compared with experimental data for magnetic framework materials. We provide several measures of the degree of frustration for each of these nets, including the ‘frustration parameter’ accessible to bulk magnetic susceptibility measurements, and the magnetic residual entropy accessible to heat-capacity measurements. We calculate the magnetic ground states, which can be measured experimentally using neutron diffraction below the magnetic ordering temperature T_N , and the spin-spin correlation functions in the spin-liquid (correlated paramagnetic) regime, which are directly accessible to neutron scattering measurements above T_N . Our results reproduce established results for well-known nets such as **crs** (pyrochlore). Importantly, however, our survey also identifies two nets that have not previously been investigated, **lcx** and **thp**, which have significant frustration as Heisenberg antiferromagnets and adopt non-collinear magnetic ground states. Moreover, we find that five nets composed of corner-sharing triangles show no order down to $T/J = 10^{-2}$ when populated with Ising spins, of which only one has been previous investigated (**crs**). These results will facilitate topology-guided synthesis and experimental identification of new magnetic materials that realise novel magnetic topologies.

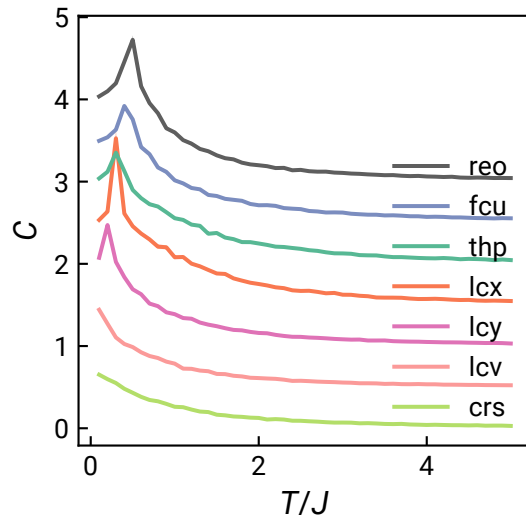


Figure 2. Heat capacity for the seven frustrated nets with nearest neighbour Heisenberg interactions derived from Monte Carlo simulations.

Table II. Ground states of the Heisenberg nearest-neighbour antiferromagnet on the high symmetry frustrated nets. The frustration parameter $f = zJ/3T_N$, and the Lacorre constraint function $L = -E/E_B$, where E is the energy per spin at $T/J = 0.1$. * This work.

	T_N/J	f	L	Ground state	\mathbf{k} -vector
crs	<0.1	>13	-0.31	Spin liquid ^{11,12}	-
fcu	0.4	10.0	-0.32	Collinear order ^{37,38}	(1,0,0)
lcv	<0.1	>13	-0.45	Octupolar order ³³	-
lcx	0.3	8.9	-0.48	120° order*	(0,0,0)
lcy	0.2	10.0	-0.46	120° order ^{32,39}	($\frac{1}{3}$,0,0)
reo	0.5	5.3	-0.47	Degenerate non-coplanar ⁴⁰	(0,0,0)
thp	0.3	8.9	-0.47	120° order*	(0,0,0)

II. RESULTS

To investigate the ground states of these models on each net, we carried out Metropolis Monte Carlo simulations on $10 \times 10 \times 10$ supercells with periodic boundary conditions, typically over the temperature range $T/J = 5$ to $T/J = 0.1$. We carried out our simulations (in moves per spin n_{MC}) for $n_{\text{MC}} = 100n_{\text{equil}}$, where n_{equil} is the number of moves require to equilibrate a spin, unless $n_{\text{equil}} > 10^5$, in which case $n_{\text{MC}} = 10^6$. Simulations were also performed for longer times on smaller systems, to check equilibration and finite-size effects.

A. Heisenberg

Of the 21 high symmetry nets, 14 are bipartite (see Supplementary Table IV).⁴¹ Since the bipartite nets order on cooling into nearest neighbour antiferromagnetic states, we do not con-

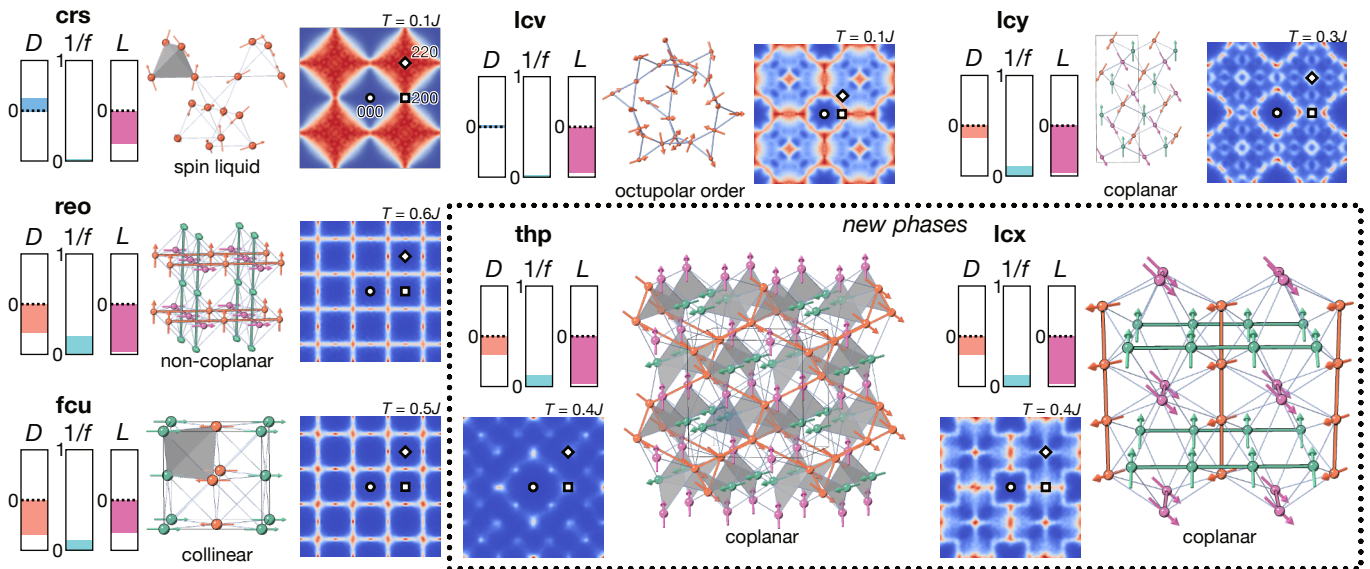


Figure 3. Summary of properties of the frustrated nets with Heisenberg spins. For each net, we show (left) three measures of the degree of frustration, defined such that larger values indicate a higher degree of frustration: D is the Maxwellian degrees of freedom defined in the text, $1/f = 3T_N/zJ$ is the inverse of the frustration parameter, and $L = -E/E_B$ is the Lacorre constraint function, where E is the energy per spin at $T/J = 0.1$. Structures shown are the ground states, with spin orientation indicated by arrows. The distinct substructures (for ordered phases) are indicated by different colours, and grey highlights show triangles or tetrahedra. Diffuse scattering in the paramagnetic phase is shown in the $hk0$ plane, and symmetrized in $m\bar{3}m$ symmetry. Temperatures of diffuse scattering calculations are labelled in each panel ($T/J = 0.1$ for phases without Néel ground states, or just above T_N for phases with Néel ground states). The (000) position is indicated by a circle, (200) by a square, and (220) by a diamond.

sider them further. Seven nets, which all have cubic symmetry, are non-bipartite: **crs** (pyrochlore), **fcu** (face-centered cubic), **lcv** (hyperkagome), **lcx** (lattice complex X), **lcy** (trillium), **reo** (octochlore) and **thp** (thorium phosphide). These nets all are frustrated and hence the magnetic ordering temperature is significantly suppressed, as indicated by the frustration parameter $f = zJ/3T_N$, where z is number of nearest neighbours. Their ground state energies E are also significantly higher than the summed absolute values of all pairwise energies E_B , as quantified by the ratio $L = -E/E_B$, which is called the Lacorre constraint function and varies between -1 (no frustration) and $+1$ (maximal frustration).⁴²

Results of our Monte Carlo simulations are summarised in Figure 3 and Table II. All seven nets ordered above $T/J = 0.1$ except **crs** (pyrochlore) and **lcv** (hyperkagome), as previously reported [Fig. 2].^{11,12,33} We note that **lcv** will also order below $T/J < 10^{-4}$ into an octupolar ground state³³. Maxwellian counting arguments^{43,44} can be used to predict the degrees of freedom per spin and hence the level of frustration: for a net comprising corner-sharing polyhedra each containing q spins with n components, assuming independence of constraints, the degree of freedom per spin $D = [n(q-2) - q]/2$. The value of D predicts that **crs** and **lcv** are the two least constrained, and hence most frustrated, nets [Fig. 3]. For the five nets that order above $T/J > 0.1$, three have been previously investigated and we reproduce these results, finding degenerate non-coplanar order in **reo**⁴⁰, collinear order in **fcu**^{37,38} and 120° coplanar order in **lcy**.^{32,39} Two nets have not previously been investigated as frustrated magnets, **lcx** and **thp**, and we discuss them further

below.

The **thp** net consists of corner-sharing triangles, and each node is connected to four different triangles, giving a coordination number of eight. This topology differs from the well-known corner-sharing triangular nets **kgm** and **lcv**, where each node is connected to two triangles, and from **lcy**, where each node connects to three triangles. The smallest non-triangle cycle in a **thp** structure is four atoms. Despite its complex appearance, **thp** is the underlying net in a number of materials; *e.g.*, it is the net formed by connecting Th atoms in Th_3P_4 —hence the name—and the actinide (Ac) cations in the broader actinide pnictides, Ac_3X_4 , $\text{X} = \text{P, As, Sb \& Bi}$. The most thoroughly characterised magnets with the **thp** net are the uranium analogues U_3X_4 , $\text{X} = \text{P, As, Sb or Bi}$.³⁶ These are metallic ferromagnets with strong local anisotropy, which produces non-collinear magnetism in U_3P_4 and U_3As_4 .⁴⁵ The **thp** net is closely related to the edge-transitive, but not vertex-transitive, **ctn** net, which consists of 3- and 4- coordinate nodes, and is widely found in MOFs and COFs^{46,47}, as it is the net formed by only considering the 4-coordinate vertices. The **thp** net therefore describes the Si net of the **ctn** topology mineral eulytite($\text{Bi}_4(\text{SiO}_4)_3$)⁴⁸ as well as the metal atom sites in the Zn-MOF MOAAF-1.⁴⁹

We found that the ground state of the Heisenberg **thp** antiferromagnet is a non-collinear 120° structure in which the three spin orientations occupy three distinct substructures, each substructure with the **dia** topology. This ordering breaks the centre of symmetry, generating a chiral structure: the highest symmetry spin structure it can adopt, with all spins lying

perpendicular to a $\langle 111 \rangle_{\text{cubic}}$ direction, has $R\bar{3}$ space group symmetry [Fig. 3].

The **l_{cx}** net, like the **thp**, is eight-coordinate and assembled from corner-sharing triangles in which each node belongs to four triangles. As previously discussed, unlike the other twenty nets considered, the shortest distance between nodes does not form an edge of the net. If only this shortest distance were to be used as an edge, the primitive rod packing (in which rods are stacked in three orthogonal directions) would be obtained.⁵⁰ There are a number of materials which contain the **l_{cx}** net, including Pt atoms in Pt₃O₄,⁵¹ and MOFs derived from the **pto** net (which is 3- and 4-coordinated), such as the Cu₂(CO₂)₄ dimers in MOF-14.⁵² We are unaware of any reports of magnetic properties of a material where magnetic ions can be considered to populate the **l_{cx}** net, although the next-nearest neighbour connections for Eu²⁺ in ferromagnetic Eu₈GaGe₃₀ would do so³¹. Like the **thp** net, the ground state of the Heisenberg **l_{cx}** antiferromagnet is a non-collinear 120° structure, in which the three spin orientations occupy three distinct substructures, in this case consisting of the 1D orthogonal chains found in the nearest neighbour net. The maximal symmetry of this ordered structure is $R\bar{3}$, again when the spins lie perpendicular to a $\langle 111 \rangle_{\text{cubic}}$ direction [Fig. 3].

For all these nets, we find that above T_N , there is significant structured magnetic diffuse scattering, indicative of strong spin-spin correlations in a cooperative paramagnet (classical spin liquid) regime [Fig. 3]. Qualitatively, the degree of structure found in the diffuse scattering is inversely related to the frustration: the more closely the diffuse scattering resembles well-defined Bragg peaks, the less frustrated the system. The degree of structure in the **l_{cx}** and **thp** diffuse scattering is consistent with the weaker frustration in these nets, compared with **crs** and **l_{cv}**.

Further insight into the frustration of these nets is provided by the interaction matrix $J(\mathbf{q})$.^{53,54} For a net with N atoms in its primitive unit cell, $J(\mathbf{q})$ is an $N \times N$ matrix with elements $J_{ij}(\mathbf{q}) = \sum_{\mathbf{R}} J_{ij}(\mathbf{R}) \exp(i\mathbf{q} \cdot \mathbf{R})$, where $J_{ij}(\mathbf{R}) \in \{0, J\}$ is the interaction between atom i in a unit cell at the origin, and atom j in the unit cell at lattice vector \mathbf{R} . In a mean-field approximation, the propagation vector of the ordered state is the wavevector (or set of wavevectors) at which the minimum eigenvalue of $J(\mathbf{q})$ is located.⁵³ For a net without frustration, the propagation vectors form a small set of symmetry-related points. By contrast, in frustrated systems, there is a degeneracy of propagation vectors. As such, the spectrum of eigenvalues of $J(\mathbf{q})$ relates the degree of frustration to the net topology, similar to the spectrum of rigid-unit-mode eigenvalues implicated in structural phase transitions of network materials⁵⁵.

Figure 4 shows the spectrum of eigenvalues of $J(\mathbf{q})$ for the seven frustrated nets. For strongly-frustrated **crs** and **l_{cv}**, the minimum eigenvalue is obtained throughout the Brillouin zone—a three-dimensional degeneracy of propagation vectors—as indicated by flat bands at minimum energy. For weakly-frustrated **fcu**, a degenerate line of propagation vectors is obtained along $\langle h10 \rangle$ and equivalent directions. We find a similar situation for **reo**, which has degenerate lines of propagation vectors along $\langle h00 \rangle$ -type directions. The degeneracy of **l_{cx}** and **l_{cy}** is two-dimensional and hence intermediate between

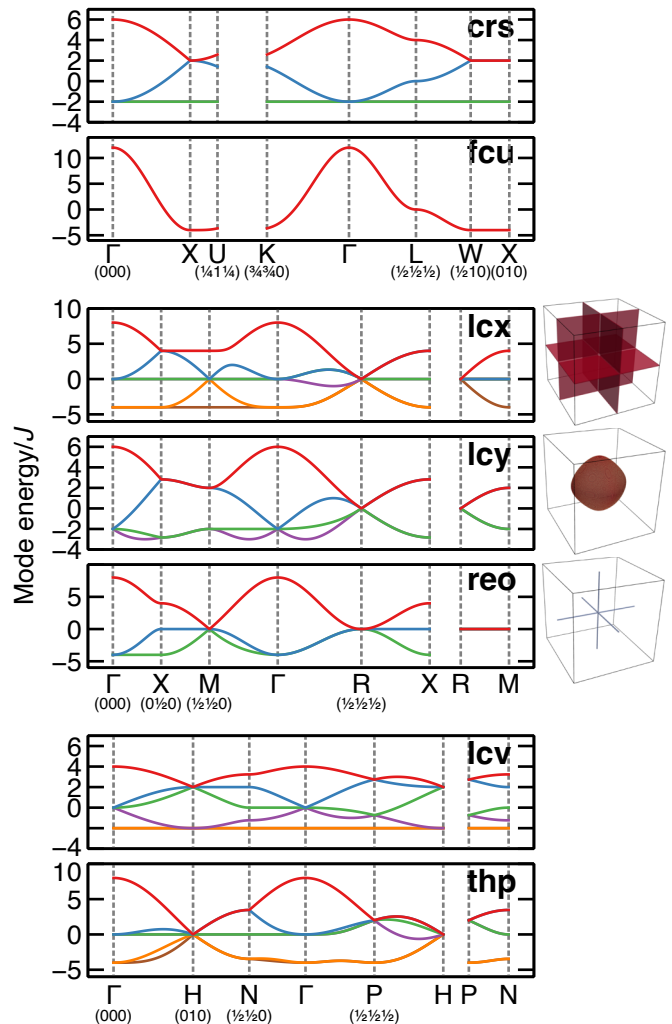


Figure 4. Dispersion of eigenvalues of the interaction matrix $J(\mathbf{q})$ for frustrated nets. For **l_{cx}**, **l_{cy}**, and **reo**, which possess primitive lattice-centering, the Brillouin zone is also shown (right) with the minimum-energy surface highlighted.

crs/l_{cv} and **fcu/reo**. For **l_{cx}**, propagation vectors are degenerate within $\{100\}$ -type planes, consistent with linear-chain correlations in real space [Fig. 3]. For **l_{cy}**, propagation vectors lie on a surface of similar $|\mathbf{q}|$ that includes the observed $(\frac{1}{3}00)$ propagation vector, reminiscent of ‘spiral spin-liquid’ phases induced by competing interactions^{22,56}. The **thp** net has two symmetry-unrelated degenerate propagation vectors, (000) and $(\frac{1}{2} \frac{1}{2} \frac{1}{2})$. While this degeneracy is zero-dimensional, there is also significant density of nearly-degenerate wavevectors with slightly higher energies [Fig. 4].

B. Ising

None of the seven frustrated nets has a collinear ground state with Heisenberg interactions. We therefore investigated how antiferromagnetic Ising spins will behave on these nets. We anticipate that the reduction in spin degrees of freedom will

Table III. Ground states of the Ising nearest-neighbour antiferromagnets. $f = zJ/3T_N$ and n_{flip}/n is the flippable spin ratio. No clear transition is seen for **reo**. * This work.

	T_N/J	f	n_{flip}/n	Ground state
crs	-	-	-	Spin liquid ⁵⁷
fcu	1.7	2.35	0	2D order ⁵⁸
lcv	$< 10^{-2}$	$> 10^2$	0.44	Spin liquid*
lcx	$< 10^{-2}$	$> 10^2$	0.25	Spin liquid*
lcy	$< 10^{-2}$	$> 10^2$	0.28	Spin liquid*
reo	?	?	0.24	Partial order ^{59,60}
thp	$< 10^{-2}$	$> 10^2$	0.22	Spin liquid*

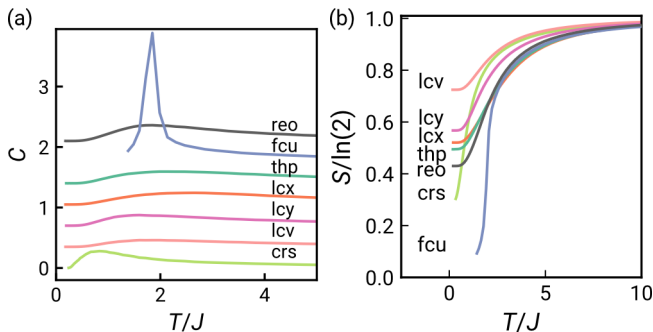


Figure 5. (a) Heat capacity, (b) magnetic entropy for frustrated nets with Ising nearest neighbour interactions.

destabilise ordered ground states, as is known for other frustrated nets in which Heisenberg spins adopt complex ordered states; notably, the Heisenberg kagome antiferromagnet orders while the Ising equivalent does not.^{7,8}

In moving from the Heisenberg to Ising spin model, we have replaced the vector spin \mathbf{S} with a binary variable S . This Hamiltonian is most likely to be realised in physical systems by binary degrees of freedom other than magnetic spin, such as site occupancy or charge,⁶¹ since the designation of a unique magnetic easy axis breaks the cubic symmetry of the net. We note that it is possible to designate local easy axes that do maintain the crystallographic symmetry—e.g., the **crs** net with local- $\langle 111 \rangle$ easy axes produces the well-known pyrochlore spin-ice model—and the effects of such anisotropy in the less well-studied nets could be of interest in future investigations.

We find, as anticipated, that reduction of the spin degrees of freedom reduces the propensity to order in these frustrated systems [Table III].⁵⁷ Out the seven vertex- and edge-transitive frustrated nets, the nearest-neighbour Ising antiferromagnet has been investigated only for three: **crs**, which does not order;⁵⁷ **fcu**, which adopts 2D order⁵⁸; and **reo**, which adopts a partial order with finite entropy^{59,60}. We reproduce these results, finding no long-range order in **crs**, a clear peak in heat capacity associated with ordering in **fcu**, and spin correlations suggestive of 2D order for **reo**, although no clear phase transition is observed. We find that the other four nets **lcv**, **lcx**, **lcy** and **thp**, which all consist of corner-sharing triangles alone, do not order down to $T/J = 10^{-2}$ with Ising spins [Table III, Fig. 5].

The magnetic entropy derived from the heat capacity reveals that there is substantial residual entropy in these four nets [Fig. 5]. A measure indicating the expected level of frustration for these nets with Ising spins can be estimated using the Pauling number,⁶² $p = (n/2^{d/2})$, where n is the number of symmetry equivalent states for each polyhedron and d is the coordination number of each polyhedron. The measure is derived from a generalisation of Pauling’s estimate for the configurational entropy of water ice, $S_{\text{config}} = R \ln(p)$.⁶² The value of p is shown in Figure 6, and correlates with the residual entropy determined through Monte Carlo simulation, with the notable exception of **crs**, which has significantly less residual magnetic entropy than the Pauling entropy would predict.

Calculation of the structure factor for each of these four nets reveals structured diffuse scattering which strongly resembles the paramagnetic diffuse scattering observed above T_N for the Heisenberg models [Fig. 6]. The acceptance ratio for each of these nets does not tend to zero even at very low temperatures ($T/J \sim 10^{-2}$), unlike the known Ising spin liquid on the **crs** net. This is due to the presence of flippable spins—spins that have equal numbers of up and down spin neighbours and hence have no net exchange field.⁶³ The acceptance ratio is therefore a measure of their concentration, and broadly agrees with the mean-field predictions (assuming all triangles have two spins ‘up’ and one ‘down’, or vice versa): $n_{\text{flip}}/n = \frac{4}{9} \approx 0.44$ for two-connected triangles; $n_{\text{flip}}/n = \frac{8}{27} \approx 0.30$ for three-connected triangles, and $n_{\text{flip}}/n = \frac{16}{81} \approx 0.20$ for four-connected triangles [Table III]. Together with the differences in structured diffuse scattering and residual entropy, the variation in this quantity is further evidence that these four spin liquid states are distinct. These four nets therefore host four classical Ising spin liquid states that, to the best of our knowledge, have not previously been investigated.

III. CONCLUSION

In this paper we have enumerated the possible magnetic states of high symmetry nets with nearest neighbour interactions. We identify that there are only seven such high-symmetry frustrated nets with nearest-neighbour Heisenberg antiferromagnetic interactions, and confirm that the only net that hosts a classical spin liquid ground state is the well-known **crs** (pyrochlore) net. We have additionally identified two nets that have not previously been investigated, **lcx** and **thp**, which have significant frustration as Heisenberg antiferromagnets and adopt non-collinear ground states. Further neighbour interactions may destabilise this 120° order and yield interesting new magnetic physics. We also predict the form of the magnetic diffuse scattering in the classical spin-liquid regime ($J > T > T_N$), which suggest significant emergent local order and facilitates future experimental identification of these states using neutron scattering.

We further investigated the behaviour of these seven frustrated nets when decorated with Ising spins. We find that five of these Ising AFMs show no order down to $T/J = 10^{-2}$, of which only one has been previously investigated (**crs**). The four corner-sharing-triangle nets we identify (**lcv**, **lcx**, **lcy** and **thp**)

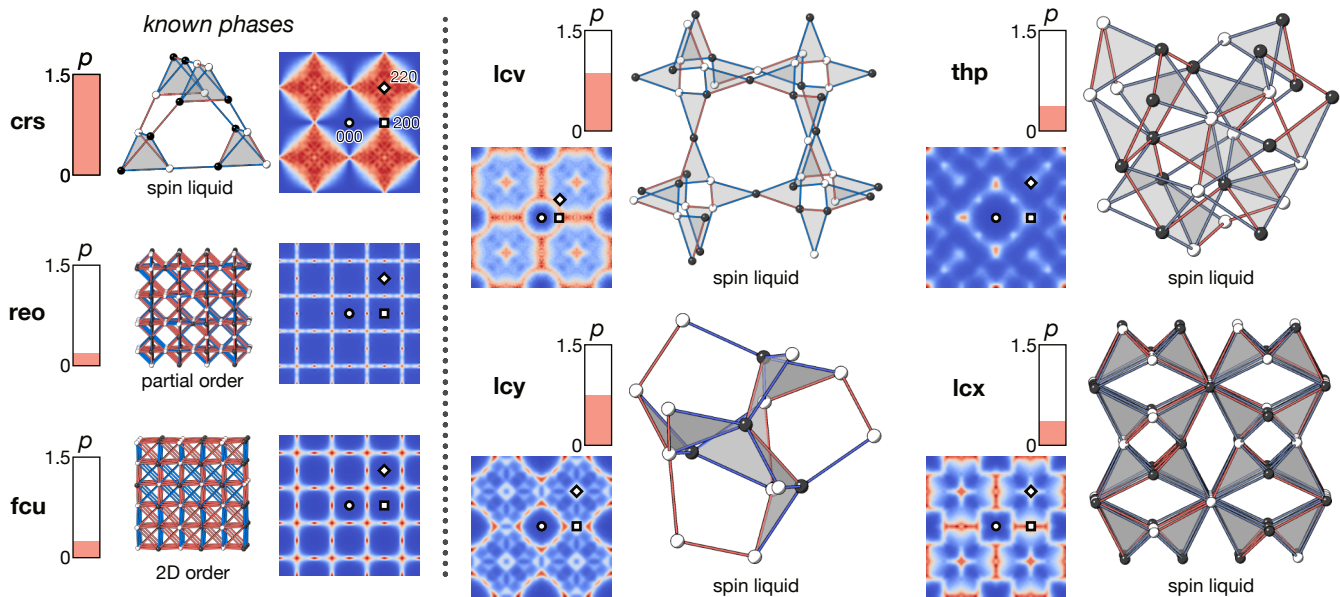


Figure 6. Summary of the properties of the frustrated nets with Ising spins. The Pauling number p is defined in the text. Structures shown with black and white colouring indicating spin direction, with red bonds indicating ferromagnetic correlation and blue bonds antiferromagnetic correlation. Grey is used to highlight triangles or tetrahedra. Diffuse scattering is calculated at $T/J = 10^{-1}$ and is shown in the $(hk0)$ plane, symmetrized in $m\bar{3}m$ symmetry. The (000) position is indicated by a circle, (200) by a square, and (220) by a diamond.

allow significant concentrations of flippable spins (*ca.* 0.3), suggestive of significant low temperature dynamics. We find that the diffuse scattering in these Ising states strongly resembles that of the Heisenberg analogues.

In this study, we have focused on the simplest combinations of interactions and nets; however, we hope that the discovery of new classical-spin-liquid states even under these constraints will spur further investigation of these models and potential materials to realise them. We now highlight a number of possible avenues for future work.

First, while we have investigated only the classical models, quantum spins are likely to facilitate the formation of more unusual states; *e.g.*, while the classical Heisenberg antiferromagnet kagome (**kgm** net) orders magnetically, the $S = \frac{1}{2}$ quantum kagome antiferromagnet is considered to have a quantum spin liquid ground state.^{8,64} More complex interactions are likely also to yield interesting states in the 13 bipartite nets; *e.g.*, Kitaev-type bond-directional interactions are predicted to produce QSL states on the **srs** (hyperoctagon or $(10,3)a$) net,⁶⁵ as well on as frustrated nets.⁶⁶ Equally, local single-ion anisotropy may transform the phases realised on these nets, even where interactions are ferromagnetic, as is known in the spin ice Coulomb phase²³. Further neighbour interactions can also ‘refrustrate’ the system and lead to disordered states that differ from the nearest-neighbour model^{24,67}. Recent work has shown that Coulomb phases can be found on other nets,

such as the ‘octochlore’ (**reo**) phase⁶⁸ or honeycomb Coulomb phase.⁶⁹ The dependence of these phases on magnetic field, whether an effective transverse field⁶³ or external field⁷⁰, is also likely to yield interesting behaviour. Finally, the success of MOF chemistry has shown that topology-guided synthesis of new materials is feasible,⁷¹ with both extensive topological databases^{17,72} and systematic design rules. We hope therefore that synthetic realisations of these phases will be achievable.

ACKNOWLEDGEMENTS

Work of M.J.C was supported by UKRI (EP/X042782/1). Work of J.A.M.P. was supported by the U.S. Department of Energy, Office of Science, Basic Energy Sciences, Materials Sciences and Engineering Division.

AUTHOR CONTRIBUTIONS STATEMENT

M.J.C. carried out the simulations. J.A.M.P. wrote the simulation software. M.J.C. and J.A.M.P. conceived the project and analysed the simulation results. M.J.C. wrote the paper, with input from J.A.M.P. .

* Electronic address: paddisonja@ornl.gov

† Electronic address: matthew.cliffe@nottingham.ac.uk

¹ C. L. Henley, *Annual Review of Condensed Matter Physics* **1**, 179 (2010).

- ² J. A. M. Paddison, H. Zhang, J. Yan, M. J. Cliffe, M. A. McGuire, S.-H. Do, S. Gao, M. B. Stone, D. Dahlbom, K. Barros, C. D. Batista, and A. D. Christianson, *npj Quantum Materials* **9**, 48 (2024).
- ³ A. P. Ramirez, *Annual Review of Materials Science* **24**, 453 (1994).
- ⁴ L. Balents, *Nature* **464**, 199 (2010), 20220838.
- ⁵ H. T. Diep, *Frustrated Spin Systems*, 2nd ed. (World Scientific, 2013).
- ⁶ C. Lacroix, P. Mendels, and F. Mila, *Introduction to Frustrated Magnetism: Materials, Experiments, Theory*, Vol. 164 (Springer Science & Business Media, 2011).
- ⁷ K. Kanô and S. Naya, *Progress of Theoretical Physics* **10**, 158 (1953).
- ⁸ J. N. Reimers and A. J. Berlinsky, *Physical Review B* **48**, 9539 (1993).
- ⁹ G. H. Wannier, *Physical Review* **79**, 357 (1950).
- ¹⁰ H. Kawamura and S. Miyashita, *Journal of the Physical Society of Japan* **53**, 4138 (1984).
- ¹¹ R. Moessner and J. T. Chalker, *Physical Review B* **58**, 12049 (1998).
- ¹² R. Moessner and J. T. Chalker, *Physical Review Letters* **80**, 2929 (1998).
- ¹³ O. M. Yaghi, M. O’Keeffe, N. W. Ockwig, H. K. Chae, M. Eddaoudi, and J. Kim, *Nature* **423**, 705 (2003), 12802325.
- ¹⁴ P. M. Bhatt, V. Guillerm, S. J. Datta, A. Shkurenko, and M. Eddaoudi, *Chem* **6**, 1613 (2020).
- ¹⁵ J. M. Bullé, J. A. M. Paddison, A. Wildes, E. Lhotel, S. J. Cassidy, B. Pato-Doldán, L. C. Gómez-Aguirre, P. J. Saines, and A. L. Goodwin, *Physical Review Letters* **128**, 177201 (2022).
- ¹⁶ V. Meschke, P. Gorai, V. Stevanović, and E. S. Toberer, *Chemistry of Materials* **33**, 4373 (2021).
- ¹⁷ M. O’Keeffe, M. A. Peskov, S. J. Ramsden, and O. M. Yaghi, *Accounts of Chemical Research* **41**, 1782 (2008).
- ¹⁸ O. Delgado-Friedrichs and M. O’Keeffe, *Acta Crystallographica A* **63**, 344 (2007).
- ¹⁹ V. A. Blatov, *Acta Crystallographica Section A: Foundations of Crystallography* **63**, 329 (2007).
- ²⁰ To the best of our knowledge there is no formal proof that these 20 nets represent the only possible vertex and edge transitive 3D nets with nearest-neighbour edges, however, extensive searches have found no others.^{18,19}
- ²¹ A. Kitaev, *Annals of Physics* **321**, 2 (2006), arXiv: cond-mat/0506438.
- ²² D. Bergman, J. Alicea, E. Gull, S. Trebst, and L. Balents, *Nature Physics* **3**, 487 (2007).
- ²³ S. T. Bramwell and M. J. Gingras, *Science (New York, N.Y.)* **294**, 1495 (2001), arxiv:cond-mat/0201427.
- ²⁴ X. Bai, J. A. M. Paddison, E. Kapit, S. M. Koohpayeh, J.-J. Wen, S. E. Dutton, A. T. Savici, A. I. Kolesnikov, G. E. Granroth, C. L. Broholm, J. T. Chalker, and M. Mourigal, *Physical Review Letters* **122**, 097201 (2019).
- ²⁵ C. G. Shull and J. S. Smart, *Physical Review* **76**, 1256 (1949).
- ²⁶ N. Khan, D. Prishchenko, Y. Skourski, V. G. Mazurenko, and A. A. Tsirlin, *Physical Review B* **99**, 144425 (2019).
- ²⁷ J. A. M. Paddison, H. Jacobsen, O. A. Petrenko, M. T. Fernandez-Diaz, P. P. Deen, and A. L. Goodwin, *Science* **350**, 179 (2015).
- ²⁸ Y. Okamoto, M. Nohara, H. Aruga-Katori, and H. Takagi, *Physical Review Letters* **99**, 137207 (2007).
- ²⁹ R. D. Blaugher, R. E. Hein, J. E. Cox, and R. M. Waterstrat, *Journal of Low Temperature Physics* **1**, 539 (1969).
- ³⁰ J. Waser and E. D. McClanahan, Jr., *The Journal of Chemical Physics* **20**, 199 (1952).
- ³¹ B. C. Sales, B. C. Chakoumakos, R. Jin, J. R. Thompson, and D. Mandrus, *Physical Review B* **63**, 245113 (2001).
- ³² J. M. Hopkinson and H.-Y. Kee, *Physical Review B* **74**, 224441 (2006).
- ³³ M. E. Zhitomirsky, *Physical Review B* **78**, 094423 (2008).
- ³⁴ C. Pfleiderer, D. Reznik, L. Pintschovius, H. v Löhneysen, M. Garst, and A. Rosch, *Nature* **427**, 227 (2004).
- ³⁵ D. Fruchart and E. F. Bertaut, *Journal of the Physical Society of Japan* **44**, 781 (1978).
- ³⁶ P. Wiśniewski, A. Gukasov, and Z. Henkie, *Physical Review B* **60**, 6242 (1999).
- ³⁷ T. Oguchi, H. Nishimori, and Y. Taguchi, *Journal of the Physical Society of Japan* **54**, 4494 (1985).
- ³⁸ R. Schick, O. Götze, T. Ziman, R. Zinke, J. Richter, and M. E. Zhitomirsky, *Physical Review B* **106**, 094431 (2022).
- ³⁹ S. V. Isakov, J. M. Hopkinson, and H.-Y. Kee, *Physical Review B* **78**, 014404 (2008).
- ⁴⁰ S. R. Sklan and C. L. Henley, *Physical Review B* **88**, 024407 (2013).
- ⁴¹ O. Delgado Friedrichs, M. O’Keeffe, and O. M. Yaghi, *Acta Crystallographica Section A Foundations of Crystallography* **59**, 515 (2003).
- ⁴² P. Lacorre, *Journal of Physics C: Solid State Physics* **20**, L775 (1987).
- ⁴³ R. Moessner and J. T. Chalker, *Phys. Rev. B* **58**, 12049 (1998).
- ⁴⁴ R. Moessner, *Canadian Journal of Physics* **79**, 1283 (2001).
- ⁴⁵ P. Burellet, J. Rossat-Mignod, R. Troć, and Z. Henkie, *Solid State Communications* **39**, 745 (1981).
- ⁴⁶ H.-X. Zhang, H.-R. Fu, H.-Y. Li, J. Zhang, and X. Bu, *Chemistry - A European Journal*, n/a (2013).
- ⁴⁷ H. M. El-Kaderi, J. R. Hunt, J. L. Mendoza-Cortés, A. P. Côté, R. E. Taylor, M. O’Keeffe, and O. M. Yaghi, *Science* **316**, 268 (2007).
- ⁴⁸ P. Fischer and F. Waldner, *Solid State Communications* **44**, 657 (1982).
- ⁴⁹ M. J. Manos, E. E. Moushi, G. S. Papaefstathiou, and A. J. Tasiopoulos, *Crystal Growth & Design* **12**, 5471 (2012).
- ⁵⁰ M. O’Keeffe and S. Andersson, *Acta Crystallographica Section A: Crystal Physics, Diffraction, Theoretical and General Crystallography* **33**, 914 (1977).
- ⁵¹ O. Muller and R. Roy, *Journal of the Less Common Metals* **16**, 129 (1968).
- ⁵² B. Chen, M. Eddaoudi, S. T. Hyde, M. O’Keeffe, and O. M. Yaghi, *Science* **291**, 1021 (2001).
- ⁵³ J. N. Reimers, A. J. Berlinsky, and A.-C. Shi, *Phys. Rev. B* **43**, 865 (1991).
- ⁵⁴ B. Canals and C. Lacroix, *Phys. Rev. B* **61**, 11251 (2000).
- ⁵⁵ L. Tan, V. Heine, G. Li, and M. T. Dove, *Reports on Progress in Physics* (2023).
- ⁵⁶ S. Gao, O. Zaharko, V. Tsurkan, Y. Su, J. S. White, G. S. Tucker, B. Roessli, F. Bourdarot, R. Sibille, D. Chernyshov, T. Fennell, A. Loidl, and C. Rüegg, *Nature Physics* **13**, 157 (2017).
- ⁵⁷ R. Liebmann, *Statistical Mechanics of Periodic Frustrated Ising Systems*, Lecture Notes in Physics (Springer-Verlag, Berlin Heidelberg, 1986).
- ⁵⁸ A. Danielian, *Physical Review Letters* **6**, 670 (1961).
- ⁵⁹ S. T. Chui, *Physical Review B* **15**, 307 (1977).
- ⁶⁰ P. Reed, *Journal of Physics A: Mathematical and General* **10**, 1745 (1977).
- ⁶¹ A. Simonov and A. L. Goodwin, *Nature Reviews Chemistry* **4**, 657 (2020).
- ⁶² A. R. Overy, A. B. Cairns, M. J. Cliffe, A. Simonov, M. G. Tucker, and A. L. Goodwin, *Nature Communications* **7**, 10445 (2016), arxiv:1508.05909.
- ⁶³ R. Moessner and S. L. Sondhi, *Physical Review B* **63**, 224401 (2001).

- ⁶⁴ L. Savary and L. Balents, *Reports on Progress in Physics* **80**, 016502 (2016).
- ⁶⁵ K. O'Brien, M. Hermanns, and S. Trebst, *Physical Review B* **93**, 085101 (2016).
- ⁶⁶ I. Kimchi and A. Vishwanath, *Physical Review B* **89**, 014414 (2014).
- ⁶⁷ P. Henelius, T. Lin, M. Enjalran, Z. Hao, J. G. Rau, J. Altsaar, F. Flicker, T. Yavors'kii, and M. J. P. Gingras, *Physical Review B* **93**, 024402 (2016).
- ⁶⁸ A. Szabó, F. Orlandi, and P. Manuel, *Physical Review Letters* **129**, 247201 (2022).
- ⁶⁹ O. Benton and R. Moessner, *Physical Review Letters* **127**, 107202 (2021).
- ⁷⁰ M. E. Zhitomirsky and H. Tsunetsugu, *Progress of Theoretical Physics Supplement* **160**, 361 (2005).
- ⁷¹ V. Guillerm and M. Eddaoudi, *Accounts of Chemical Research* **54**, 3298 (2021).
- ⁷² V. A. Blatov, A. P. Shevchenko, and D. M. Proserpio, *Crystal Growth & Design* **14**, 3576 (2014).

A. SI Figures

Table IV: Complete list of nets investigated.

label	z	Bipartite	space group
acs	6	Y	$P6_3/mmc$
ana	4	Y	$Ia\bar{3}d$
bcu	8	Y	$Im\bar{3}m$
bcs	6	Y	$Ia\bar{3}d^*$
crs	4	N	$Fd\bar{3}m$
dia	4	Y	$Fd\bar{3}m$
fcu	12	N	$Fm\bar{3}m$
hcg	6	Y	$Pn\bar{3}m^*$
lcs	4	Y	$Ia\bar{3}d$
lcv	4	N	$I4_132$
lcx	8	N	$Pm\bar{3}n^\dagger$
lcy	6	N	$P4_132$
lvt	4	Y	$I4_1/amd$
nbo	4	Y	$Im\bar{3}m$
pcu	6	Y	$Pm\bar{3}m$
qtz	4	Y	$P6_222$
reo	8	N	$Pm\bar{3}m$
rhr	4	Y	$Im\bar{3}m$
sod	4	Y	$Im\bar{3}m$
srs	3	Y	$I4_132$
thp	8	N	$I\bar{4}3d$

* cannot use distance criterion † not nearest neighbour

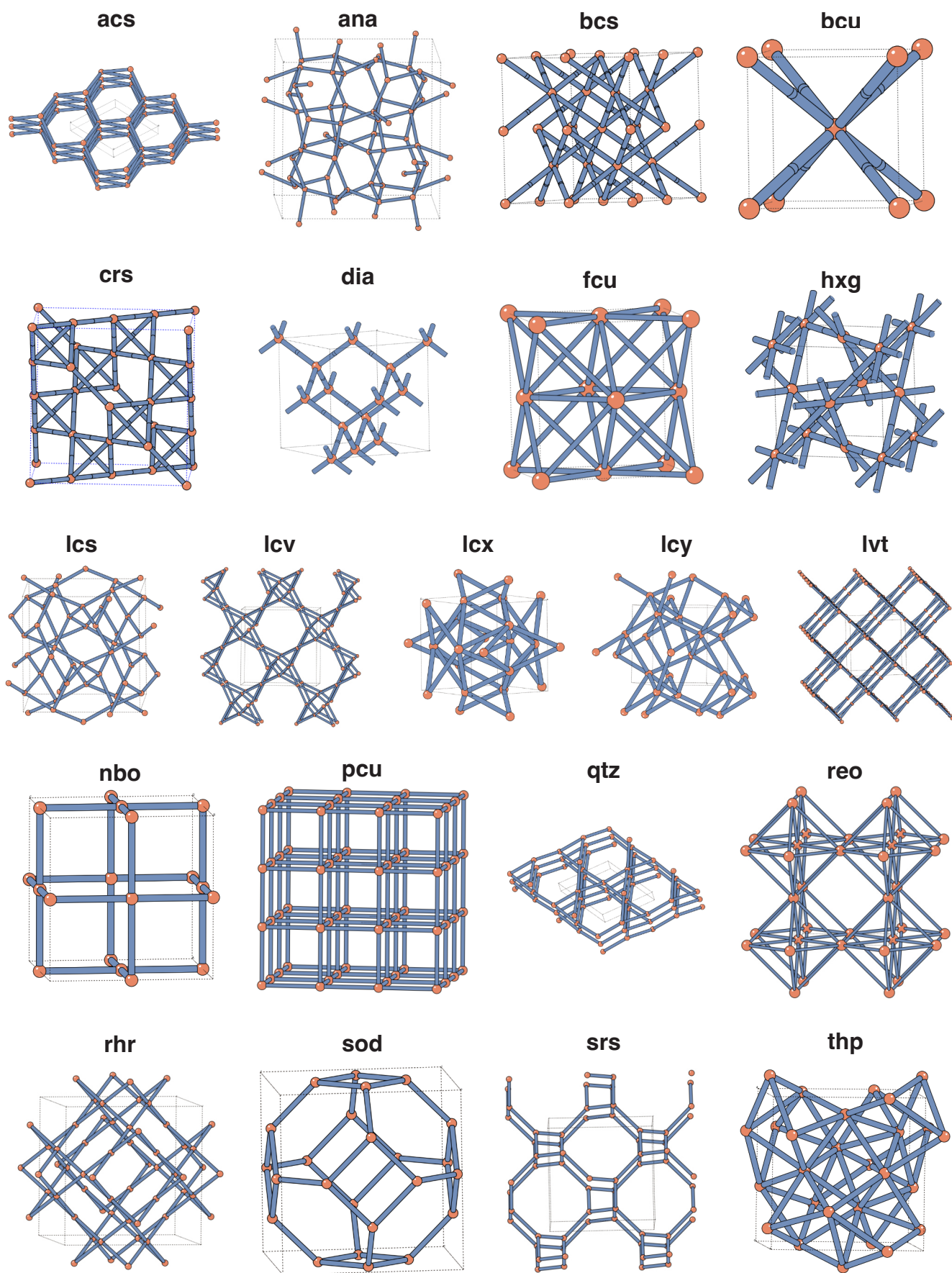


Figure 7. SI Fig: Summary of all edge and vertex transitive nets.